ISSN 1392–1207. MECHANIKA. 2022 Volume 28(5): 401–409

Cemented Carbide Layer Thickness Optimization of Carbide Anvil Based on Thermodynamic Coupling

Guizhong XIE*, Tao WANG*, Liangwen WANG*, Xiaoyun GONG*, Shixin ZHANG*, Zeheng ZHI*, Ziyong ZHAO, Xiaojun YANG****

**Henan Key Laboratory of Mechanical Equipment Intelligent Manufacturing, Mechanical and Electrical Engineering Institute, Zhengzhou University of Light Industry, Zhengzhou 450002, China,*
E-mails: wangtao617@126.com, w_liangwen@sina.com
***Henan Huanghe whirlwind Co.. LTD, Changge, 461500, China, E-mail: 1642741831@qq.com*

crossref http://dx.doi.org/10.5755/j02.mech.30808

1. Introduction

As the hardest substance in nature, diamond has a series of excellent physical and chemical properties, especially in cutting and polishing tools. It is estimated that about 98 % of industrial grade diamonds use artificial diamonds [1-2]. Because diamond has high hardness, good thermal conductivity, wear resistance and excellent light transmittance and corrosion resistance, etc. it is widely used in the electronic industry. However, in actual production, fatigue crack is easy to occur in carbide anvil system, which leads to fracture phenomenon in the cubic synthetic diamond press [3-4], thus the quality and output of diamond is affected. In order to improve the quality of diamond, the development of high-performance the cubic synthetic diamond press and the corresponding carbide anvil system has become the primary task of the artificial diamond industry in all countries [5-6].

Through finite element simulation, Han Q. G. et al [7]. obtained the properties and shear stress distribution of cemented carbide in cubic-anvil high pressure apparatus (SPD-6 2000). The results show that to avoid the fatigue failure of anvil, the maximum shear stress of WC anvil with 8 % cobalt content shall be less than 3.17 GPa, which provides a good basis for evaluating the properties of cemented carbide anvil. Zhang Y. et al. simulated the stress distribution with and without support ring by finite element method. The conclusion is drawn that two kinds of tungsten carbide opposite anvils have been manufactured with bevelled angle of 10. A good design basis for the structural improvement of the carbide anvil has been put forward [8]. However, these works only consider the simulation results under the stress field, and the influence of high temperature on the carbide anvil is neglected. Importing the carbide anvil model into the finite element, the stress distribution of the carbide anvil system is obtained by Zhou X. J. et al. It is *401*nalyses that it was liable to fracture on the edge of top surface under high pressure status [9]. The influence of the main parameters of the carbide anvil on the stress is *401*nalyses by finite element method. By discussing the optimum value of structural parameters, a new type of jacking carbide anvil structure is proposed [10]. However, only the size of carbide anvil without considering the fit size in the assembly is optimized, which means that other parts will change with the anvil size, resulting in a decrease in fit accuracy.

The method in this paper considers the influence of temperature on carbide anvil system. The matching size of the carbide anvil system is set to the same variable parameters to ensure the matching accuracy. This paper *401*nalyses the temperature distribution of the whole carbide anvil system by means of finite element method. On the basis of temperature analysis, thermodynamic coupling analysis was carried out to obtain the stress distribution. In this paper, an optimization design based on thermodynamic coupling is proposed, and the simulation values of stress and temperature, which affect the fatigue failure of carbide anvil, are taken as the target variables. The service life of carbide anvil can be improved by reducing the stress and temperature. The research of this paper provides a good theoretical basis for the analysis of carbide anvil fracture, the improvement of the service life of the carbide anvil and the design criteria of the carbide anvil.

The research contents of this paper are as follows. The second chapter introduces the three-dimensional modelling of the carbide anvil system and the finite element analysis of the temperature field. In chapter 3, the distribution of contact stress and shear stress of carbide anvil system in the coupled field with or without load is introduced, respectively. The fourth chapter introduces the optimization of the carbide layer thickness of carbide anvil based on the analysis of thermodynamic coupling simulation. The conclusions are drawn in the last chapter.

2. Steady-state thermal analysis and principle of carbide anvil system

The internal environment of carbide anvil system is subjected to high temperature and high pressure [11]. The carbide anvil system at high temperature is prone to large deformation. The stress distribution of that is affected due to the thermal expansion of the material. Under this poor working conditions, the failure of the anvil may be accelerated, which may lead to the anvil cracking in the synthetic cavity. And the quality of the diamond is affected. Therefore, it is necessary to analyze the carbide anvil system and consider the temperature distribution.

Thermodynamics is a common physical problem, through which the temperature distribution inside a structure can be obtained. ANSYS Workbench has two thermal analysis methods. One is steady-state thermodynamic analysis, the other is transient thermodynamic analysis. Steady-state thermodynamic analysis is adopted in this paper, the principle of which is as follows [12-14]:

$$[\boldsymbol{K}]\{\boldsymbol{I}\} = \{\boldsymbol{Q}\}, \tag{1}$$

where: $[K]$ is the conduction matrix; $\{I\}$ is the temperature vector of the node, and $\{Q\}$ is the heat flow vector of the node.

There are three forms of heat transfer, heat conduction, heat convection and heat radiation. The heat transfer form of anvil is mainly heat conduction, which can be expressed as:

$$\Phi = -\lambda A \frac{\partial T}{\partial x}, \quad (2)$$

wWhere: Φ is the heat flow rate; A is the area of the carbide anvil surface; λ is the thermal conductivity of the material; T is the temperature, and x is the coordinate axis perpendicular to the interface.

$$\rho c \frac{\partial T}{\partial t} = \frac{\partial}{\partial x}\left(\lambda \frac{\partial T}{\partial x}\right) + \frac{\partial}{\partial y}\left(\lambda \frac{\partial T}{\partial y}\right) + \frac{\partial}{\partial z}\left(\lambda \frac{\partial T}{\partial z}\right) + \Phi, \quad (3)$$

where: ρ is the density of the material; c is the specific heat capacity; t is the time, and λ_x, λ_y, λ_z is the thermal conductivity of the material in the x, y and z directions.

In the thermal analysis, the temperature load is applied to each element node by interpolation method, and the temperature function of the element is determined as follows:

$$T^e(x,y,z) = N(x,y,z) \bullet q_T^e. \quad (4)$$

In the process of steady-state heat transfer, the temperature load remains unchanged. The element heat transfer matrix equation can be obtained by combining the element temperature field function with the boundary conditions of steady-state heat transfer, as shown in formula (5):

$$\boldsymbol{K}_T^e \bullet \boldsymbol{q}_T^e = \boldsymbol{P}_T^e, \quad (5)$$

where: $\boldsymbol{K}_T^e$ is the heat transfer matrix of element; $\boldsymbol{q}_T^e$ is the temperature matrix of element node, and $\boldsymbol{P}_T^e$ is the equivalent temperature load matrix of element node.

2.1. Finite element modeling of thermal analysis of carbide anvil system

Import the carbide anvil system model of 3D modeling software SolidWorks into finite element software. Each part is shown in Fig. 1 The carbide anvil system assembly is comprised of a carbide anvil, a steel ring and a cushion block. The workbench working interface in ANSYS is used to build the thermal analysis platform. The model is imported into finite element software for temperature field analysis.

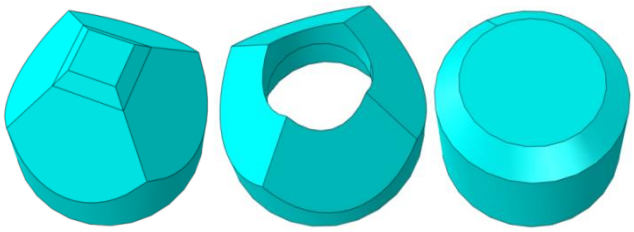

a) Carbide anvil b) Steel ring c) Cushion block

Fig. 1 Parts of carbide anvil system

2.2. Material properties of carbide anvil system

The working environment of the carbide anvil is subjected to high temperature and high pressure. Because the cemented carbide material has the advantages of high strength, high thermal strength and good corrosion resistance, the top material of the carbide anvil uses YG8 cemented carbide. The carbide anvil's body, steel ring and cushion block are made of low alloy ultrahigh strength steel 45CrNiMoNA [15]. Stratified carbide anvil is shown in Fig. 2.

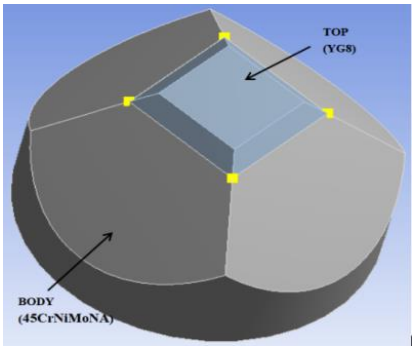

Fig. 2 Carbide anvil stratification

The related parameters of the two materials are shown in Table 1.

Table 1

Material parameter of YG8 and 45CrNiMoNA

Material	Density, kg/m^3	Thermal conductivity, W/m^2·°C	Thermal expansivity, m/k	Elastic modulus, Pa	Poisson ratio
YG8	15000	75.4	4.5×10^{-6}	6×10^{11}	0.22
45CrNiMoNA	7900	20	14.5×10^{-6}	2.01×10^{11}	0.3

2.3. Determination of temperature loading boundary conditions

In practical work, the cubic synthetic diamond press is subjected to at a high temperature and high-pressure environment. In our method, the carbide anvil top surface is subjected to a temperature load of 200℃. In addition, in order to reduce the high temperature of the steel ring, a counter flow cooling device is applied, the temperature is 85℃, and the flow heat transfer coefficient is 1000 W/m^2·°C. The bevel to steel ring and carbide anvil 's incline is in direct contact with the air, which also removes some of the heat. Thus, set the heat transfer coefficient with the air to 20 W/m^2·°C.

2.4. Compared with the temperature field of traditional carbide anvil system

The thermal analysis of the carbide anvil system is used to simulate the temperature distribution in actual operation. Due to the high temperature environment, the temperature gradient is obvious and the carbide anvil will produce thermal deformation when heated, resulting in thermal expansion force and accelerating the failure of the carbide anvil [16].

The carbide anvil used in this paper is divided into two parts. The top layer of carbide anvil is made of hard alloy YG8, and the body is made of low-alloy ultra-high strength steel 45CrNiMoNA. Because the thermal conductivity of cemented carbide YG8 is higher than 45CrNiMoNA, the thermal insulation effect is better. Therefore, the temperature ranging of the top layer of cemented carbide layered carbide anvil is larger than that of traditional carbide anvil. Similarly, the temperature gradient and low temperature area of stratified carbide anvil are smaller than those of without stratified carbide anvil, as shown in Fig. 3. This can better provide a stable, high temperature contact temperature for diamond manufacturing, and better simulate the diamond forming environment.

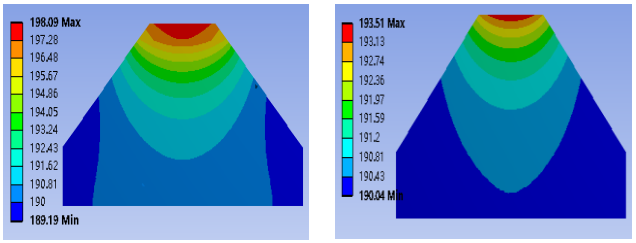

a) Stratified b) Without stratified

Fig. 3 temperature distribution

2.5. Temperature field of carbide anvil system

As can be seen from the simulated temperature distribution diagram, the maximum temperature at the center of carbide anvil top surface is 198.09℃. It is in good agreement with the actual measured temperature of 200℃ [17]. From the path defined in Fig. 4a and Fig. 5a, it can be seen that the temperature gradually increases from the diagonal point to the center point, and the temperature gradually decreases from the center point to the diagonal point on the other side. From the path defined in Fig. 4b and Fig. 5b, it can be seen that the temperature gradually decreases with the increase of the distance from the carbide anvil top surface to the bottom surface. This is due to the main heat source applied to the carbide anvil top surface, heat transfer along the axis, the decreasing temperature. In addition, the temperature of the inclined surface of carbide anvil is lower than that of the carbide anvil top surface because the heat dissipation of the inclined surface is faster in contact with the air.

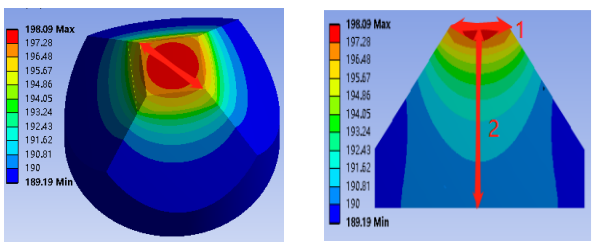

a) Overall b) Section

Fig. 4 Carbide anvil temperature distribution

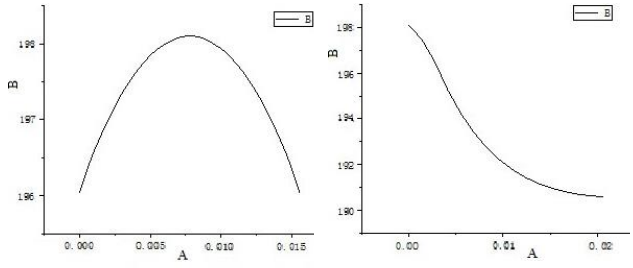

a b

Fig. 5 Temperature curve of path: a) Path 1; b) Path 2

2.6 Temperature field of steel ring and cushion block

The maximum temperature of the steel ring is 107.27 ℃ because the large slope is in contact with the air, which takes away some of the heat, as shown in Fig. 6. In addition, the water flow at the lower end of the steel ring can also take away some heat, thus the temperature of the steel ring bevel and cylindrical surface is much smaller than that of the contact surface of carbide anvil and cushion block. Due to the small volume of carbide anvil and cushion block, and the cushion block in contact with carbide anvil, the temperature loss is less. Thus the temperature distribution of cushion block is relatively concentrated, without obvious temperature gradient, and the temperature is kept at about 190℃ when it reaches a stable equilibrium, as shown in Fig. 7.

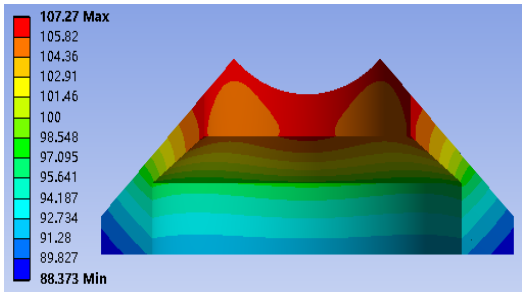

Fig. 6 Temperature distribution of steel ring

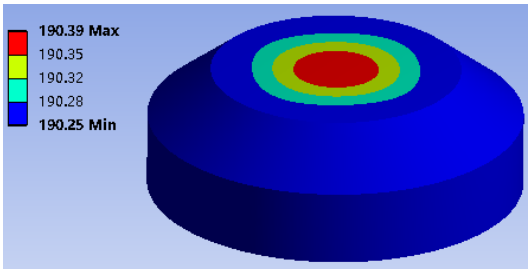

Fig. 7 Temperature distribution of cushion block

3. Analysis and principle of carbide anvil stress under thermodynamic coupling

In order to study the influence of thermal expansion force of materials on carbide anvil system under high temperature environment [18-21], the pretightening force of carbide anvil on steel ring and cushion block on steel ring under no load is simulated. The simulation results of temperature field are introduced into the stress field to simulate the pretightening force of each contact surface under the condition of no load and temperature. The influence of temperature on anvil system is analyzed by comparing the pretightening force between the two cases. Besides, the stress

field analysis of the carbide anvil also determines the life and strength of the carbide anvil system in the working environment.

The coupling mode adopted in this paper is thermal indirect unidirectional coupling, and the finite element analysis equation is based on the physical equation of temperature analysis and virtual work principle.

1. Physical equation of thermal stress. Due to the existence of temperature difference $\Delta T(x, y, z)$ inside the structure, the structure produces expansion $\alpha_T \cdot \Delta T(x, y, z)$; α_T is the thermal expansion coefficient of the material). The physical equation of thermal stress can be obtained by introducing thermal expansion into the structural physical equation [22]:

$$\begin{cases} \varepsilon_{xx} = \dfrac{1}{E}\left[\sigma_{xx} - \mu\left(\sigma_{yy} + \sigma_{zz}\right)\right] + \alpha_T \bullet \Delta T \\ \varepsilon_{yy} = \dfrac{1}{E}\left[\sigma_{yy} - \mu\left(\sigma_{xx} + \sigma_{zz}\right)\right] + \alpha_T \bullet \Delta T \\ \varepsilon_{zz} = \dfrac{1}{E}\left[\sigma_{zz} - \mu\left(\sigma_{xx} + \sigma_{yy}\right)\right] + \alpha_T \bullet \Delta T \\ \gamma_{xy} = \dfrac{1}{G}\tau_{xy}, \gamma_{yz} = \dfrac{1}{G}\tau_{yz}, \gamma_{zx} = \dfrac{1}{G}\tau_{zx} \end{cases}. \tag{6}$$

2. Virtual work principle. The traditional virtual work principle for analyzing elastic problems is [23]:

$$\delta U - \delta W = 0. \tag{7}$$

The thermal stress analysis and the elastic problem adopt the same virtual work principle (as shown in formula (6), (7) and (8)), which is converted into matrix form, and combined with the physical equation of thermal stress, the thermal analysis virtual work equation is obtained:

$$\int_{\Omega} \sigma_{ij}\ \delta\varepsilon_{ij}\ d\Omega - \left(\int_{\Omega} \overline{b_i}\ \delta u_i\ d\Omega + \int_{\Omega} \overline{P_i}\ \delta u_i\ dA\right), \tag{8}$$

$$\sigma_{ij} = D_{ijkl}\left(\varepsilon_{kl} - \varepsilon_{ij}^{o}\right), \tag{9}$$

$$\boldsymbol{\varepsilon}_{ij}^{o} = \left[\alpha_T\ \Delta T \alpha_T\ \Delta T \alpha_T\ \Delta T\right]^T. \tag{10}$$

Substitute Formula (4) into Formula (6) to obtain the thermal analysis virtual work equation:

$$\int_{\Omega} D_{ijkl}\left(\varepsilon_{kl} - \varepsilon_{kl}^{o}\right)\delta\ \varepsilon_{ij} d\Omega - \left(\int_{\Omega} \overline{b_i}\ \delta u_i\ d\Omega + \int_{S_p} \overline{P_i}\ \delta u_i\ dA\right). \tag{11}$$

In addition, the displacement matrix of element node in finite element is shown in Eq. (10):

$$\boldsymbol{q}^e = \left[u_1 \quad v_1 \quad w_1 \quad \ldots \quad u_n \quad v_n \quad w_n\right]^T. \tag{12}$$

The relationship of element node displacement is used to represent the basic mechanical parameters of the element, as shown in Formulas (11) and (12), and the finite element formula of structural stress considering the influence of temperature is shown in Formula (13):

$$\boldsymbol{u} = \boldsymbol{N}\boldsymbol{q}^e, \tag{13}$$

$$\boldsymbol{\varepsilon} = \boldsymbol{B}\boldsymbol{q}^e, \tag{14}$$

$$\sigma = Sq^e - D \bullet \alpha_T\ \Delta T\left[1 \quad 1 \quad 1 \quad 0 \quad 0 \quad 0\right]^{\mathrm{T}}, \tag{15}$$

where: N is the shape function matrix; B is the geometric matrix; D is the elastic coefficient matrix, and S is the stress matrix.

3.1. Analysis of pretightening force of steel ring

As shown in Fig. 8, the pretightening force of steel ring without load and temperature influence is shown. The contact stress of the steel ring is distributed unevenly due to the steel ring is cut from a cylindrical material at an angle of 46°, and the part which wraps the carbide anvil is thinned when the material is removed. The maximum pretightening force is 852.6 MPa. The analysis results of temperature field are imported into the analysis of stress field, and the results are shown in Fig. 9. The maximum stress is 1005 MPa. Compared with the pretightening force under the condition without load, the pretightening force is increased by about 17.9%, thus it can be seen that the temperature will lead to the thermal deformation of the material and produce thermal expansion force, which affects the stress of the carbide anvil system.

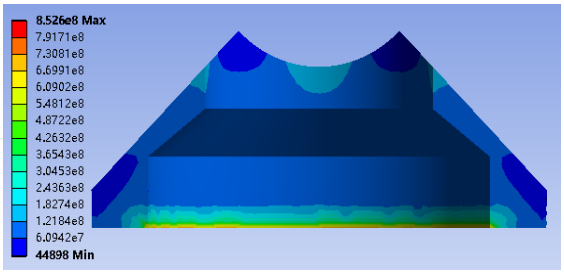

Fig. 8 Pretightening force of steel ring without load

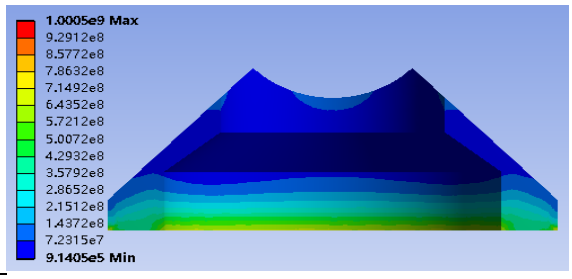

Fig. 9 Pretightening force of steel ring under temperature load

3.2. Stress analysis of carbide anvil under temperature load

The analysis results of temperature field are imported into the stress field without boundary conditions for analysis. The simulation results are shown in Fig. 10 and Fig. 11. It can be seen that the carbide layer of the carbide anvil has the greatest contact stress with its body. This is because that the thermal expansion coefficients of the two materials are very different, resulting in the two parts of the force not the same. The thermal expansion force of cemented carbide YG8 is greater than that of low alloy ultra-

high strength steel 45CrNiMoNA. Thus the stress of the carbide layer is greater than that of the carbide anvil body. Similarly, under the joint action of contact stress and temperature load, maximum shear stress appears on the four edges and corners of the carbide anvil top surface, and the distribution of shear stress is symmetrical on the diagonal.

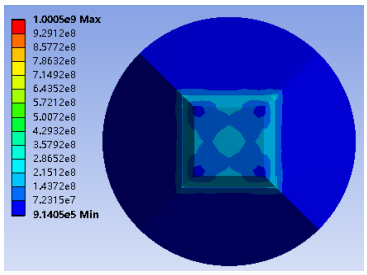

Fig. 10 carbide anvil under temperature load

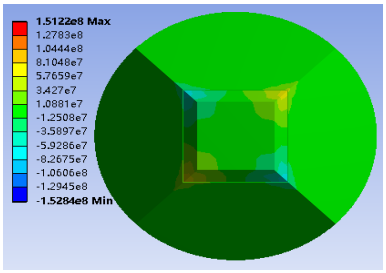

Fig. 11 Shear stress of carbide anvil top surface under temperature load

3.3. Analysis of simulation results under thermodynamic coupling

Based on the previous temperature field analysis results, the simulation results are imported into the stress field and the corresponding boundary conditions are added to analyze the coupling field. In the actual process of diamond production, the carbide anvil is subjected to the high pressure P_1=1 GPa on the carbide anvil top surface of the synthetic cavity. Applied the positive pressure P_2 of the gasket on the carbide anvil small slope, and the friction force f of the composite block on the small slope. A fixed constraint is applied to the bottom of the carbide anvil system, and the load distribution of the carbide anvil is shown Fig. 12 [24].

1. The positive pressure on the small inclined plane is:

$$P_2 = P_1 \cdot e^{\frac{2vs}{t}}. \tag{16}$$

2. The friction force received by the small inclined plane is:

$$f = \varepsilon \cdot P_2, \tag{17}$$

where: v is the internal friction coefficient of pyrophyllite; s is the local coordinates of the four angles of carbide anvil, and t is the thickness of sealing pad and the external friction coefficient of pyrophyllite to carbide anvil, respectively.

The stress of coupled field carbide anvil system after applying boundary conditions is shown in Figs. 13-14.

It can be seen that the carbide anvil system is more affected by temperature than before, and the stress after thermodynamic coupling generally increases a lot due to the generation of thermal expansion force [25]. Because the material of the carbide anvil of the cubic synthetic diamond press is a brittle material, the fatigue failure of brittle material is mainly shear failure caused by shear stress. Therefore, the distribution of shear force is emphasized in the analysis of carbide anvil. The comparisons between Fig. 15 show that the shear force increases a lot under the influence of temperature, and the shear stress concentrates near the four prisms. In practical work, fatigue failure and crack are easy to occur near the four edges and corners of carbide anvil [26]. As shown in Fig. 14a the crack location of the anvil is the same as the simulation result, which proves the accuracy of the simulation result from the side. The simulation results also explain the fact that the service life of the carbide anvil under temperature load is lower than that without temperature load.

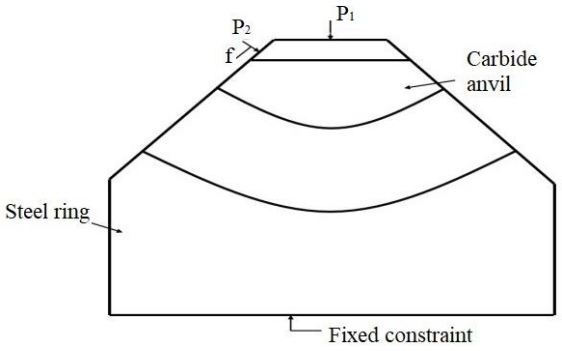

Fig. 12 Boundary conditions of anvil system

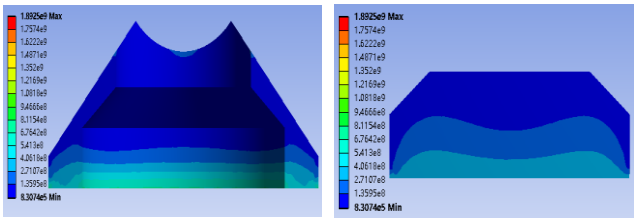

a) Steel ring b) Cushion block

Fig. 13 Stress diagram under thermodynamic coupling

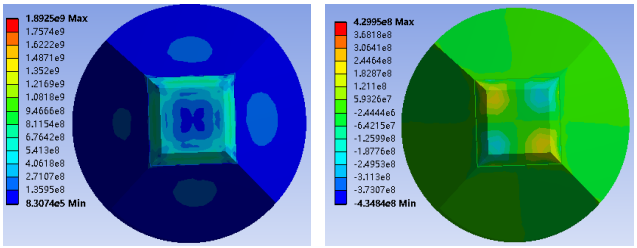

a) Contact stress diagram b) Shear stress diagram

Fig. 14 The result of carbide anvil under thermodynamic coupling

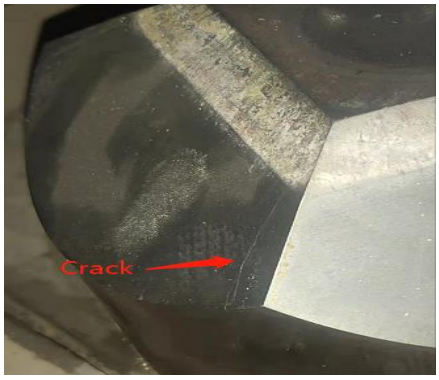

Fig. 15 Partial enlarged view of crack location

4. Optimize the thickness of cemented carbide layer of carbide anvil

Because the cemented carbide layer thickness can affect the carbide anvil stress distribution, stable stress can better simulate the diamond forming conditions in natural environment for graphite. Therefore, it is very important to determine the optimal thickness of cemented carbide layer for producing high quality diamond.

Kriging model is an optimal linear unbiased estimation method [27-29], which estimates unknown functions by weighted average of known functions, and its prediction theory is close to linear regression. The Kriging model is constructed by selecting the appropriate covariance function and estimating the objective function.

The formula of Kriging model is:

$$y(x) = g(x)^T \beta + Z(x), \tag{18}$$

where: $y(x)$ is the response function; $g(x)$ is the basis function; β is the regression coefficient; $z(x)$ is the normal distribution function, and x is the relevant experimental variable. In addition, the expectation, variance and covariance of the normal distribution function $z(x)$ are represented by E, VAR and COV, respectively.

$$\begin{cases} E[z(x)] = 0 \\ VAR[z(x)] = \sigma^2 \\ COV[z(w), z(x)] = \sigma^2 R(w, x, \theta) \end{cases}, \tag{19}$$

where: σ^2 is the variance; θ is the unknown correlation parameter; $R(w, x, \theta)$ is the correlation function between w and x.

The predicted value of the design variable is expressed as:

$$\hat{y} = g(x)^T \hat{\beta} + r(x)^T R^{-1}(Y - x\hat{\beta}), \tag{20}$$

where: $\hat{y}$ is the predicted value; $\hat{\beta}$ is the estimated value of regression coefficient; R is the correlation matrix; $r(x)$ is the relationship vector between unknown points and known points, and Y is the output value of regression data.

4.1. Sensitivity analysis of carbide anvil size

In the 3D software SolidWorks, a parametric model is established according to the dimensions of carbide anvil system, and the basic dimensions are imported into the finite element software, and the associated dimensions are established with the software. Taking the dimensions of carbide anvil system as input variables, the mass, maximum temperature, maximum contact and shear stress are defined as target variables. The sensitivity analysis of carbide anvil size parameters is carried out in order to find out the parameters that have a greater impact on the target variables [30-33]. In order to ensure that there will be no interference when the size of parts changes, the same fitting size of each part is expressed by the same variable parameter. The $P_2 \sim P_8$ dimensions of the carbide anvil system are shown in Fig. 16. The $P_9 \sim P_{13}$ successively represent the carbide anvil mass, average temperature, maximum contact and shear stress of carbide anvil, respectively. Fig. 17 shows the correlation coefficients between input variables and target variables. It can be seen that the influential parameters of anvil are width of carbide anvil P_6, height of carbide anvil P_8 and thickness of cemented carbide layer P_4.

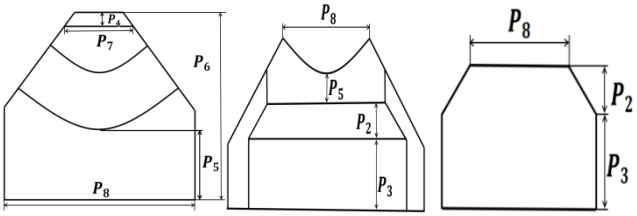

a) Carbide anvil b) Steel ring c) Cushion block

Fig. 16 Dimensioning of carbide anvil assembly parts

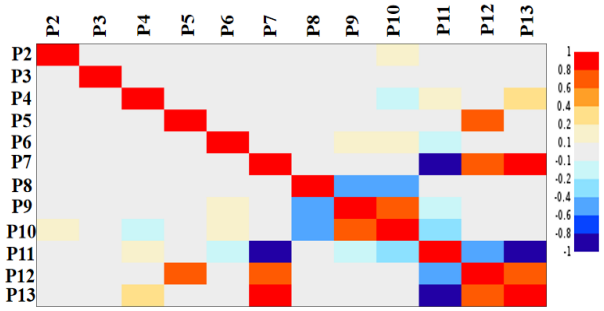

Fig. 17 Correlation matrix diagram

4.2. Response surface Construction

In this paper, the upper and lower 20 % variation values of each size of carbide anvil system are selected as the parameter variation range, and the Kriging model is selected for optimization. In this paper, the Optimal Space-filling Design (OSF) method is used to design sample points within the feasible domain consisting of the value range of Design variables. The advantage of OSF is that the selected sample points are distributed more evenly in the space, and the extremum problem is solved more effectively, providing better coverage for the design space and ensuring the filling of the design space [34].

In software Solidworks, the model is parameterized and then imported into workbench optimization module. In the end, a total of 50 groups of design variables and sample points of contact stress, shear stress and temperature were designed, as shown in Table 2.

Table 2

Sample points obtained in DOE experiment

Design point	*P*4	*P*8	*P*9, Pa	*P*10, Pa	*P*11, °C
1	1.988	18.76	1.8356E9	3.3916E8	192.11
2	2.02	19.08	1.8199E9	3.7171E8	206.02
3	2.084	20.04	1.6162E9	2.7896E8	214.24
49	1.876	18.92	1.8238E9	3.732E8	188.52
50	1.836	21.08	1.5269E9	3.0298E8	187.34

Kriging surrogate model is used to construct response surface and establish the relationship between input variables and output variables. Select 40 groups from the sample points for the training of the surrogate model, and set 10 groups of verification points to verify the calculation results of the design points. Figs. 18, a, b and c shows the response surfaces of P4 and P8 on contact stress, shear stress and temperature, respectively. Fig. 18, a show that the contact stress fluctuates with the increase of P4 and P8. It can be seen from Figs. 18 b and c that with the increase of P4 and P8, the shear stress and temperature are also gradually increasing, but the growth rate of Fig. 18, c is slow.

As shown in Fig. 19, the design points and verification points under this model can be well fitted near a straight line, indicating that the fitting accuracy of the response surface meets the requirements and verifying the feasibility of the established proxy model. The Kriging model is suitable for the optimization calculation in this paper.

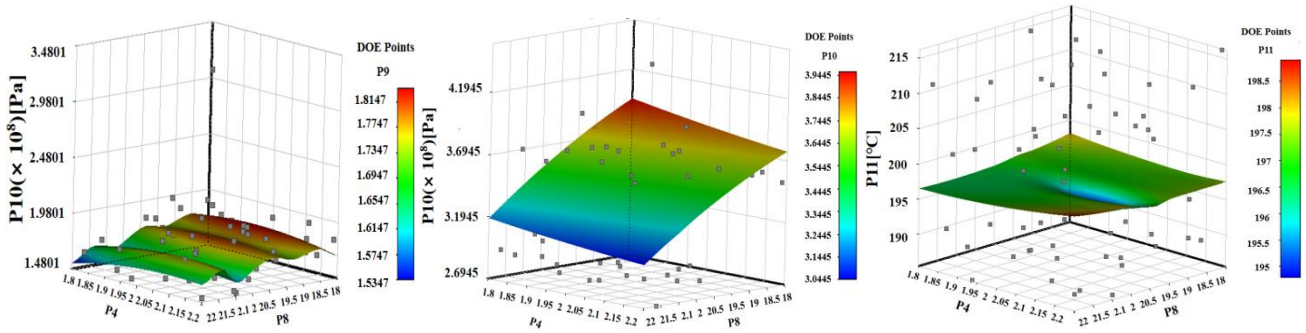

a) Response surfaces to contact stress b) Response surfaces to shear stress c) Response surfaces to temperature

Fig. 18 Response surfaces of P4 and P8 to contact stress, shear stress and temperature respectively

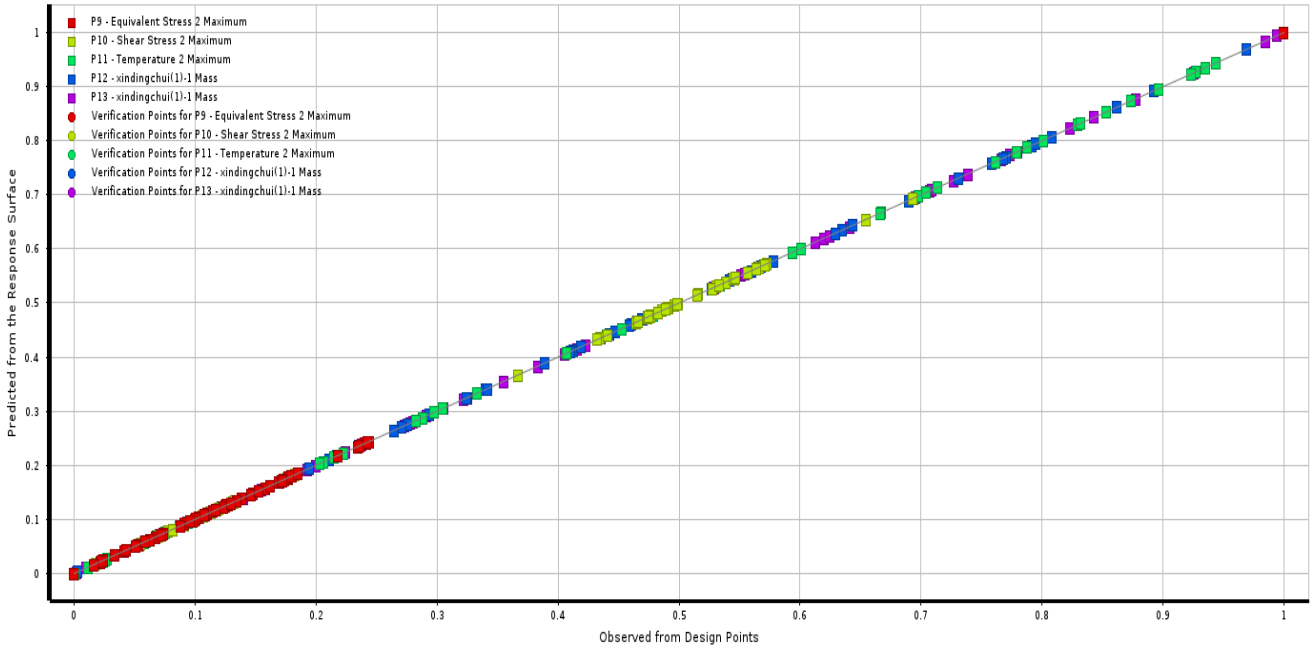

Fig. 19 The design points and verification points fitting curve

4.3. Analysis of optimization results

The optimization simulation uses the previous calculation results of thermodynamic coupling to bring different sample points into the constructed coupling field for calculation again. Until the calculation is complete, choose the best result. The optimization results are shown in Table 3.

Before optimization, the maximum contact stress is 1.7805GPa, the maximum shear stress is 0.37445 GPa, and the maximum temperature is 198.09 ℃. After optimization, the results show that the thickness of cemented carbide layer is 1.8 cm, the maximum contact stress is reduced by 387.5 MPa, the maximum shear stress is reduced by 110.55 MPa, and the temperature is decreased by 10.11℃.

Table 3

The optimized results

Thickness of cemented carbide layer, cm	Maximum contact stress, Pa	Maximum shear stress, Pa	Maximum Temperature, ℃
1.8	1.393E9	2.6390E8	187.98
1.8324	1.403E9	2.9282E8	186.25
1.8945	1.531E9	2.8202E8	187.79

In this paper, finite element method is used to simulate carbide anvil system under the action of temperature field and stress field. The analysis results show that in the temperature field, the highest temperature at the center point of the carbide anvil surface is 198.09℃, and the whole carbide anvil presents a temperature gradient distribution. The temperature distribution of the steel ring is not uniform, and the temperature of the cushion block is close to 190℃ approximately, which is almost the same as the temperature of the carbide anvil. Due to the influence of thermal expansion, the contact stress of steel ring increases by 17.9 % under the action of temperature field. In the analysis of coupling field, the shear force is concentrated near the four edges of carbide anvil, and fatigue cracks are easy to occur. This is consistent with the crack location of carbide anvil in practice, which proves the accuracy of simulation results. Because the carbide anvil system is fixed at the bottom, the stress is greatest at the bottom. In the optimization analysis, in the 20 % change above and below each size, when the thickness of cemented carbide layer is 1.8 cm, the optimum stress results are obtained. The research of carbide anvil system in this paper has important practical significance for improving the service life of carbide anvil and designing the size of carbide anvil.

Funding

This work was partly supported by the National Natural Science Foundation of China (52075500), partly supported by the Key Scientific Research Projects of Institutions of Higher Learning in Henan Province (21A460029 and 21A460030), and by Key Scientific Project of Henan Province (211110220200 and 212102210313).

References

1. **Wang, H.; Zhu, D.; Zou, C. M.** et al. 2012. Evolution of the microstructure and nanohardness of Ti–48 at. % Al alloy solidified under high pressure, Materials and Design 34: 488-493. https://doi.org/10.1016/j.matdes.2011.08.030.
2. **Yu, G.; Han, Q. G.; Li, M. Z.** et al. 2012. Finite element analysis of the high-pressure tungsten carbide radius-anvil, Acta Physica Sinica 61(4): 273-335.
3. **Zhou, X. J.; Xu, Z. W.; Chen, R. Q.** et al. 2014. Coupled thermal analysis on carbide anvil of cubic press, Advanced Materials Research 852: 629-633.
4. **Singh, A. K.; Divakar, C.; Mohan, M.** 1983. Step-loading technique for tungsten carbide opposed anvil high-pressure setup, Review of Scientific Instruments 54(10): 1407-1409.
5. **Han, Q. G.; Zhang, Q.; Li, M. Z.** et al. 2012. An effective solution for the best set of beveling parameters of the cubic high-pressure tungsten carbide anvil, Chin. phys. lett 29(11): 116201. https://doi.org/10.1088/0256-307X/29/11/116201.
6. **Yang, J.; Chen, B.; Wang, Y.; Wang, C. Z.** 2020. Crack detection in carbide anvil using acoustic signal and deep learning with particle swarm optimisation, Measurement 173: 108668. https://doi.org/10.1016/j.measurement.2020.108668.
7. **Han, Q. G.; Jia, X. P.; Jia, X. P.; Qin, J. M.** et al. 2014. Finite-element analysis on performance and shear stress of cemented tungsten carbide anvils used in the China-type cubic-anvil high-pressure apparatus, High Pressure Research 29(3): 457-465. https://doi.org/10.1080/08957950903170373.
8. **Zhao, Y.; Chen, X. P.** et al. 2014. Optimization of tungsten carbide opposite anvils used in the in situ high-pressure loading apparatus, Mathematical Problems in Engineering 10(11): 1-5. https://doi.org/10.1155/2014/607520.
9. **Zhou, X. J.** 2014. Coupled thermal analysis on carbide anvil of cubic press, Advanced Materials Research 8(52): 629-633. https://doi.org/10.4028/www.scientific.net/AMR.852.629.
10. **Wang, Q.; Cai, D. M.; Zhao, D.** 2004. Structure optimization on carbide anvil of BELT apparatus, Heavy machinery 19(1): 53-57.
11. **Sterer, E.; Silvera, I. F.** 2006. The c-DAC: A novel cubic diamond anvil cell with large sample volume area and multidirectional optics, Review of Scientific Instruments 77(11): 115105. https://doi.org/10.1063/1.2387890.
12. **Mouffak, E.; Bouchetara, M.** 2016. Transient thermal behavior of automotive dry clutch discs by using Ansys software, Mechanika 22(6): 562-570. https://doi.org/10.5755/j01.mech.22.6.17277.
13. **Guo, X. P.; Han, W. Y.** 2013. The numerical simulation analysis of tuyere's temperature field and stress field, Advanced Materials Research 706-708: 1701-1704. https://doi.org/10.4028/www.scientific.net/AMR.706-708.1701.
14. **Al-Merbati, A. S.** et al. 2013. Thermodynamics and thermal stress analysis of thermoelectric power generator: Influence of pin geometry on device performance, Applied Thermal Engineering 50(1): 683-692. https://doi.org/10.1016/j.applthermaleng.2012.07.021.
15. **Ikhlef, N.; Mekideche, M. R.** et al. 2011. Modeling of analysis ICP torch at atmospheric pressure with applied voltage, IEEE Transactions on Plasam Science 39(11): 2380-2381. https://doi.org/10.1109/TPS.2011.2163733.
16. **Singh, A. K.** 2003. Uniaxial stress component in tungsten carbide anvil high ressure x-ray cameras, Journal of Applied Physics 45(11): 4686.
17. **Han, Q. G.; Yang, W. K.** et al. 2014. Hybrid-toroidal anvil: a replacement for the conventional WC anvil used for the large volume cubic high-pressure apparatus, High Pressure Research 34(4): 404-411. https://doi.org/10.1080/08957959.2014.971785.
18. **Peng, W.** 2017. Research on preparation method of fine grained cemented carbide anvil with WC/Co nano composite powder, Superhard Material Engineering 29(5): 17-24.
19. **Peng, W.** et al. 2013. Application of advanced technology of cemented carbide in manufacturing large size anvil, Superhard Material Engineering 25(1): 25-29.
20. **Narvydas, E.** et al. 2021. Application of finite element sub-modeling techniques in structural mechanics, Mechanika 27(6): 459-464. https://doi.org/10.5755/ j02.mech.25962.
21. **Xie, N.; Zhang, Z.** et al. 2017. Power losses and thermodynamic analysis of the solenoid fuel injector, International Journal of Applied Electromagnetics and Mechanics 54.3 (2017): 405-419.

https://doi.org/10.3233/JAE-150143.
22. **Wei, K. X.** et al. 2019. Modeling and analysis of thermal coupling between power devices, IEEE Transactions on Electron Devices 66(10): 4302-4308. https://doi.org/10.1109/TED.2019.2936618.
23. **Song, H.; Hou, G.** et al. 2015. Rigid–elastic-thermal coupling dynamics and its application, Advances in Mechanical Engineering 7(12): 168781. https://doi.org/10.1177/1687814015619766.
24. **Han, L.; Chen, B.; Gao, B. C.** et al. 2013. Fault detection of carbide anvil based on hurst exponent and BP neural network, Advanced Materials Research 805-806: 1881-1886. https://doi.org/10.4028/www.scientific.net/AMR.805-806.1881.
25. **Qi, X. D.; Shen, X. L.** 2015. Multidisciplinary design optimization of turbine disks based on ANSYS workbench platforms, Procedia Engineering 99(1): 1275-1283. https://doi.org/10.1016/j.proeng.2014.12.659
26. **Panda, P. C.; Ruoff, A. L.** 1979. The relation of the yield stress of high-pressure anvils to the pressure attained at yielding and the ultimate attainable pressure, Journal of Applied Physics 50(2): 582-588.
27. **Klei, jnen. J. P. C.** 2014. Simulation-optimization via Kriging and bootstrapping: a survey, Journal of Simulation 8(4): 241-250. https://doi.org/10.1057/jos.2014.4.
28. **Sakata, S. I.; Ashida, F.; Zako, M.** et al. 2002. Structural optimization using Kriging approximation, Computer methods in applied mechanics and engineering 192(7-8): 923-939. https://doi.org/10.1016/S0045-7825(02)00617-5.
29. **Sakata, S. I.; Ashida, F.; Zako, M.** 2008. Approximate structural optimization using kriging method and digital modeling technique considering noise in sampling data, Computers and Structures 86(13-14): 1477-1485. https://doi.org/10.1016/j.compstruc.2007.05.007.
30. **Osakabe, T.; Kakurai, K.; D, Kawana.** et al. 2007. Development of a hybrid-anvil type high-pressure device and its application to magnetic neutron scattering studies, Journal of Magnetism & Magnetic Materials 310(2): 2725-2727. https://doi.org/10.1016/j.jmmm.2006.10.959.
31. **Toal, D. J. J.** 2015. A study into the potential of GPUs for the efficient construction and evaluation of Kriging models, Engineering with Computers 32(3): 377-404. https://doi.org/10.1016/10.1007/s00366-015-0421-2.
32. **Nair, A.; Kumanan, S.** 2018. Optimization of size and form characteristics using multi-objective grey analysis in abrasive water jet drilling of Inconel 617, Journal of the Brazilian Society of Mechanical Sciences and Engineering 40(3): 121. https://doi.org/10.1007/s40430-018-1042-7.
33. **Nguyen, T.; Vu, T. C.** et al. 2020. Multi-responses optimization of fnishing honing process for surface quality and production rate, Journal of the Brazilian Society of Mechanical Sciences and Engineering 42(11): 604. https://doi.org/10.1007/s40430-020-02690-y.
34. **Wang, L.** 2010. Nondestructive Testing Method of Cemented Carbide Anvil Based on Stress Analysis, Cemented Carbide 27(2): 107-109.

G. Z. Xie, T. Wang, L. W. Wang, X. Y. Gong, S. X. Zhang, Z. H. Zhi, Z. Y. Zhao, X. J. Yang

CEMENTED CARBIDE LAYER THICKNESS OPTIMIZATION OF CARBIDE ANVIL BASED ON THERMODYNAMIC COUPLING

S u m m a r y

This paper presents cemented carbide layer thickness optimization of a carbide anvil based on thermodynamic coupling analysis. In our method, the established carbide anvil system through SolidWorks is firstly imported into the finite element software. The temperature field and thermal-mechanical coupling field of the carbide anvil system are analyzed. From the simulation results, it can be found that the contact stress of steel ring under temperature load is increased by 17.9% compared with that without temperature load. Thus, the service life of carbide anvil under temperature load is lower than that without temperature load. In addition, the four edges of anvil are prone to fatigue cracks due to the phenomenon of shear stress concentration. This is consistent with the actual crack location of cemented carbide anvil, which verifies the accuracy and rationality of thermal-mechanical coupling simulation. The thickness of cemented carbide layer is optimized based on thermodynamic coupling. The optimization results show that the thickness of 1.8 cm is the best when size ranges from 1.8 cm to 2.2 cm. The maximum contact stress, the maximum shear stress, the temperature is all reduced by 387.5 MPa, 110.55 MPa, and 10.11℃, respectively.

Keywords: Thermodynamic coupling, carbide anvil, optimization, cemented carbide layer.

Received February 27, 2022
Accepted October 17, 2022